Droplet Distribution Spectrum Effects on Dry Ice Growth on Cylinders

*Pavlo Sokolov & Muhammad S.Virk
Institute of Industrial Technology,
UiT – The Arctic University of Norway
*Email: pavlo.sokolov@uit.no

ABSTRACT

A detailed parametric analytical study along with a series of viscid multiphase numerical simulations of ice accretion were performed in comparison with experimental data of ice accretion on a 30 mm diameter cylinder. The study was performed for droplet distribution spectra, *Langmuir (A-J)*, in addition to an experimental droplet distribution obtained in an icing tunnel. Analysis shows that droplet distribution spectrum has a pronounced effect on cloud impingement parameters, such as droplet overall collision efficiency (E), droplet local collision efficiency (β_0), droplet maximum impingement angle (θ), droplet impact velocity (V_0), accreted ice mass and density. The values of these parameters can significantly change at the same operating conditions and median volume diameter (MVD) with a change of droplet distribution spectrum. These differences are more pronounced at low values of droplet inertia parameter, (*K)*. Further experimental, analytical and numerical investigations into those aspects at lower values of droplet inertia parameter are deemed necessary in order to expand the understanding of different cloud impingement parameters on the ice accretion process and performance of current icing theory in cases with low values of K. For the low values of *K*, which correspond to the values of $E \leq 0.10$, the use of the full droplet spectrum is recommended in calculations instead of monodispersed. In addition, based on the results of this and previous works the Langmuir D distribution is recommended as standard or "first guess" distribution.

Keywords: ice accretion; cylinder; collision efficiency; droplet distribution spectrum; MVD; CFD.

1. Introduction

The interest in modeling ice accretion on cylindrical objects primarily comes from preventing structural damage or collapse of objects such as overhead transmission lines or communication masts due to the accreted ice mass leading to dynamic instabilities. Ice mass accretion in these cases primarily comes from atmospheric icing such as in-cloud or precipitation icing. In studying these one prime interest lies in the parameterization of characteristics of in-cloud droplet impingement on cylinders. The study of in-cloud icing is not a new scientific field with some major milestones in terms of mathematical models being works by (Langmuir and Blodgett, 1944), (Cansdale and McNaugthon, 1977), (Lozowski et al., 1979), (Stallabrass, 1980), (Makkonen, 1984) and (Finstad et al., 1988a). The latter being independently verified by (Stallabrass and Makkonen, 1987) serves as a current benchmark model for atmospheric icing and it is part of governing standard ISO:12494 "*Atmospheric Icing of Structures*" (ISO, 2001). The core of the Finstad et al. model uses a so-called "Median Volume Diameter approximation" (MVD) in order to parameterize the in-cloud droplet spectrum using a singular value and an assumption that the cloud droplet distribution can be adequately represented using a uniform droplet distribution, where all the droplets have the same diameter, corresponding to cloud MVD. The verification of the concept was carried out by Finstad in the doctoral thesis (Finstad, 1986), later expanded in paper of (Finstad et al., 1988b) and based on the results of (Makkonen and Stallabrass, 1987) it can be stated that the Finstad et al. model is applicable for the ranges of droplets overall collision efficiencies of $0.07 < E < 0.63$.

Jones (Jones et al., 2014) showed that MVD approximation may not always be valid and in natural conditions such as on Mt. Washington in USA, the use of a droplet distribution spectrum can yield significantly better results over a monodisperse distribution when comparing ice accretion data on a multicylinder device. ISO 12494 standard states that the Finstad et. al model has a tendency to under estimate the overall collision efficiency for cases, when $E < 0.10$. Recently, (Makkonen et al., 2018) shown that modern Computational Fluid Dynamics (CFD) tools can achieve good results in modeling of ice accretion on cylinders for cases when $E < 0.10$, granted full droplet distribution spectrum is used. When it comes to estimating the cloud impingement parameters of ice accretion, $X(K, \varphi)$, those parameters depend on the droplet inertia parameter (*K)* and Langmuir parameter φ, which are defined as (ISO, 2001):

$$K = \frac{\rho_p d_p^2 u}{18 \mu_f c} \tag{1}$$

$$\varphi = \frac{Re^2}{K} \tag{2}$$

where ρ_p is droplet (water) density, u is the freestream wind speed, μ_f is air density, c is the characteristic length of the object, being radius in case of a cylinder and d_p is the droplet MVD. When it comes to calculations of droplet impingement parameters using full droplet distribution spectrum, one can see that:

$$K_{spec} = \sum w_i K_i \tag{3}$$

$$X(K, \phi)_{spec} = \sum w_i X(K_i, \phi)_i \tag{4}$$

where w_i is fractional weight of bin i, subscript i refers to a given parameter calculated for bin i, while subscript *spec* shows spectrum averaged values. The spectrum values are linearly dependent on the per-bin values, as spectrum values, $X(K, \varphi)_{spec}$ are obtained by summation of per-bin values $X(K_i, \varphi)_i$ using LWC fraction w_i as a weighting constant. Conversely, per bin values are dependent as square of bin's MVD, and independent of φ as it can be seen from the structure of it in eq. (2). Such dependence may result in a significant change of cloud impingement parameter values, when droplet distribution spectrum is changed, even in the case where different droplet distributions have matching MVD value of the entire spectrum. This study aims to address; the impact of different droplet distribution spectra with matching MVDs on the ice accretion process, the changes of the key model parameters, introduced by the change of droplet distribution spectra and some of the aspects of utilizing some simplistic constraints and performance of modern CFD software for multiphase numerical simulations of low wind speed in-cloud icing events.

Recently, (Makkonen et al., 2018) performed a series of CFD simulations using the full droplet distribution spectrum. However, unlike their work, which used Lagrangian specification of flow field, current work utilizes the Eulerian specification of flow field, which will be detailed in subsequent sections. The main reason for choosing the Eulerian formulation is that the majority of previous studies, mentioned earlier in this section, have used the Lagrangian flow formulation. It is deemed worthwhile to investigate how the Eulerian flow formulation used in CFD will perform in the modeling of the ice accretion process. Finally, one of the prime practical applications of the approaches used in this study is the possible improvement in ice load maps generation, using mesoscale modeling in WRF/NWP, particularly if the assumed droplet distribution spectra, given in subsequent section, can be implemented in the WRF/NWP model. Again, the practical application here is generating the ice load maps for the wind power and power transmission industries.

2. Design of the Experiment

In this study, the icing tunnel experiments were performed with the focus on low values of K. A 30 mm rotating cylinder at wind speed of 4 m/s was chosen for in-depth parametric and numerical investigation. The rotation of cylinder has been chosen in order to keep the results easily transferable to the ISO 12494 (ISO, 2001) procedure of estimated ice loads, in addition, to keeping in line with assumption (Makkonen, 1984) of slowly rotating iced power lines, which are assumed to be the prime object in ice load maps generation. The operating conditions for this test case are given in Table 1. The conditions chosen should be typical of a dry growth condition, thus the sticking and freezing efficiencies are assumed to be equal to unity.

Parameter	Value
Cylinder diameter (mm)	30
Cylinder length (mm)	157
Air velocity (m/s)	4
Air temperature (°C)	–5
Altitude (m.a.s.l)	10
Icing duration (min)	30
LWC (g/m^3)	0.4
Rotational speed (RPM)	5

Table 1. Icing tunnel experiment conditions.

The parametric study is done via the analytical calculations, using the Finstad et al. model (Finstad et al., 1988a) for the calculation of overall collision efficiency (E), stagnation line droplet local collision efficiency (β_0), maximum impingement angle (θ) and stagnation line droplet impact velocity (V_0) and density. While the impact of the overall collision efficiency on

the ice accretion process is straightforward enough, as the accreted ice mass is directly dependent on it, via the "Makkonen model" formulation (Makkonen, 2001), the impact of other cloud impingement parameters is just as important. These parameters directly affect the physical properties of the accreted ice, such as density, which is a function of droplet impact velocity via Macklin formulation (Macklin, 1962) and ice deposit shape, which is a function of local collision efficiency and the impingement angle (Lozowski et al., 1983), (Finstad, 1986). These cloud impingement parameters can alter the ice accretion process, especially for the long-term icing events, as by altering the shape and density of deposit, the values of the droplet inertia parameter K will change, which will result in further changes to the values of the cloud impingement parameters.

The formulation of (Makkonen, 1984) is used for the analytical calculation of accreted ice density, cylinder surface temperatures and iced cylinder diameter change at each time step. The numerical modeling is done via a series of viscid CFD simulations using Reynolds-Averaged Navier-Stokes (RANS) equations. These simulations are performed on a rotating cylinder. In both cases, the droplet distribution in the icing tunnel, as provided by VTT Technical Research Centre of Finland is used. This droplet distribution is given in Figure 1. The calculated MVD of this distribution is 18.73 microns.

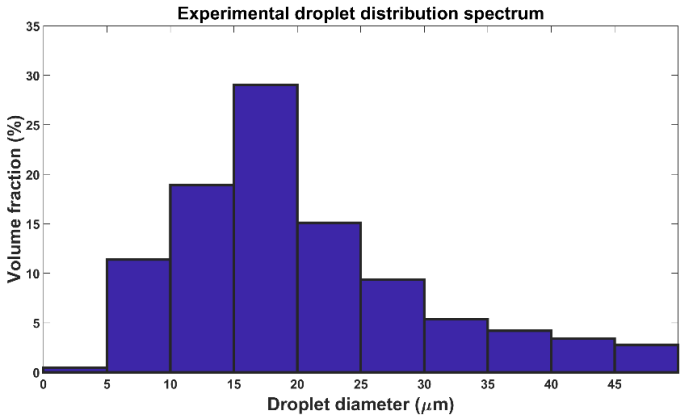

Figure 1. Experimental droplet distribution spectrum.

Moreover, in order to study the effect of droplet distribution on the ice accretion process different parameterizations of the droplet spectrum, namely the gamma distributions (also referred as Langmuir distributions) are used (Howe, 1990). The gamma distributions used in this study are given in Table 2 in terms of diameter ratios. All gamma distributions have MVD of 18.73 with 'distribution A' being monodispersed. These droplet distributions progressively get "wider" as the ratio of diameters increases, meaning that for distributions with higher value of diameter ratios, the diameters of bins will become progressively smaller or larger, when compared with "preceding" distribution. For the droplet spectrum, each bin collision efficiency is calculated independently and then weighted using the LWC fraction, in order to obtain the overall collision efficiency of the entire spectrum.

LWC fraction	A	B	C	D	E	F	G	H	J
0.05	1.00	0.56	0.42	0.31	0.23	0.18	0.13	0.10	0.06
0.1	1.00	0.72	0.61	0.52	0.44	0.37	0.32	0.27	0.19
0.2	1.00	0.84	0.77	0.71	0.65	0.59	0.54	0.50	0.42
0.3	1.00	1.00	1.00	1.00	1.00	1.00	1.00	1.00	1.00
0.2	1.00	1.17	1.26	1.37	1.48	1.60	1.73	1.88	2.20
0.1	1.00	1.32	1.51	1.74	2.00	2.30	2.64	3.03	4.00
0.05	1.00	1.49	1.81	2.22	2.71	3.31	4.04	4.93	7.34

Table 2. Langmuir distributions.

The Langmuir distributions B–E were initially presented in (Langmuir and Blodgett, 1944) as a mathematical approximations of the droplet distribution spectra in fog and rising clouds on Mt. Washington observatory. Later, (Howe, 1990) presented "wider" droplet distributions F–J, based on previous observations on Mt. Washington observatory, in order to adequately capture bimodal and trimodal droplet distributions, which are expected to happen in nature.

2.1 Analytical Model

The cloud impingement parameters are calculated in accordance to (Finstad et al., 1988a) as:

$$X(K,\phi) = \left[C_{X,1}K^{C_{X,2}}\exp\left(C_{X,3}K^{C_{X,4}}\right) + C_{X,5}\right] - \left[C_{X,6}(\phi - 100)^{C_{X,7}}\right] \times \left[C_{X,8}K^{C_{X,9}}\exp\left(C_{X,10}K^{C_{X,11}}\right) + C_{X,12}\right] \quad (5)$$

where X is either the overall collision efficiency E, the stagnation line collision efficiency β_0, the maximum impingement angle α_{max}, or the non-dimensional impact velocity V_0. The constants $C_{X,n}$ are listed in Table 3.

Coefficient	$X = \beta_0$	$X = \alpha_{max}$	$X = E$	$X = V_0$
$C_{X,1}$	1.218	2.433	1.066	1.030
$C_{X,2}$	-6.70×10^{-3}	-4.70×10^{-3}	-6.16×10^{-3}	1.68×10^{-3}
$C_{X,3}$	–0.551	–0.375	–1.103	–0.796
$C_{X,4}$	–0.643	–0.576	–0.688	–0.780
$C_{X,5}$	–0.170	–0.781	–0.028	–0.040
$C_{X,6}$	3.05×10^{-3}	8.50×10^{-3}	6.37×10^{-3}	9.44×10^{-3}
$C_{X,7}$	0.430	0.383	0.381	0.344
$C_{X,8}$	2.220	1.757	3.641	2.657
$C_{X,9}$	–0.450	–0.298	–0.498	–0.519
$C_{X,10}$	–0.767	–0.420	–1.497	–1.060
$C_{X,11}$	–0.806	–0.960	–0.694	–0.842
$C_{X,12}$	–0.068	–0.179	–0.045	–0.029

Table 3: Coefficient values of cloud impingement parameters (Finstad et al., 1988a).

The ice deposit diameter D_i of cylinder is calculated as (Makkonen, 1984):

$$D_i = \left[\frac{4(M_i - M_{i-1})}{\pi\rho_i} + D_{i-1}^2\right]^{1/2} \quad (6)$$

Where M is the mass accretion value per unit length, ρ is the ice density and subscript i indicates the time step. In all analytical calculations the time step used is, t =12 seconds. This is to ensure that the cylinder rotates at least 360° degrees along its longitudinal axis on each time step to ensure even ice deposit on the surface, in accordance with (Makkonen, 1984). The accreted ice density at any given time step is calculated as (Makkonen, 1984).:

$$\rho_i = 378 + 425\log_{10}(R_m) - 82.3\left(\log_{10}(R_m)\right)^2 \quad (7)$$

where, R_m is the Macklin density parameter, given as:

$$R_m = -\frac{V_0 d}{2t_s} \quad (8)$$

Where d is the MVD in microns, V_0 is the impact velocity of the droplet in m/s and t_s is the surface temperature of the ice deposit in Celsius. In the case of dry growth the surface temperature of the ice deposit can be obtained numerically as:

$$\frac{2}{\pi}Evw\left(L_f + c_w t_a - c_i t_s\right) = h\left[(t_s - t_s) + \frac{kL_s}{c_p p_a}(e_s - e_a) - \frac{rv^2}{2c_p}\right] + \sigma\alpha(t_s - t_s) \quad (9)$$

where L_f and L_s are latent heats of fusion and sublimation respectively, c_w, c_i, and c_p are specific heats of water, ice and air respectively, p_a, e_s and e_a are air pressure, saturation water vapour pressures at surface and air temperatures respectively, h is the overall heat transfer coefficient, k = 0.62, r is the recovery factor, with value of 0.79 being used for cylinder, t_s and t_a are surface and air temperatures in Celsius, σ is the Stefan-Boltzmann constant and $\alpha = 8.1 \times 10^7$ K^3. More details on the terms of heat transfer and derivation of heat transfer equations are given in (Makkonen, 1984).

2.2 Experimental Setup

The experiments were conducted in the VTT icing wind tunnel. This is an "open-loop" tunnel placed entirely inside a large cold room. The cross-section of the tunnel mouth is 0.7m by 0.7m. Ice was accumulated on 0.157m long smooth aluminium cylinder, 30mm in diameter, placed vertically and rotated by a motor at a constant 5 RPM. The schematic of the icing wind tunnel is given in Figure 2. To rule out the effect of blockage, the cylinder was located in front of the exit of the tunnel. The temperature and wind speed in the test section were measured using calibrated sensors. The liquid water content (LWC) was calibrated for each wind speed and temperature pair by measuring the ice growth on a 30mm cylinder and using the formulas defined in ISO 12494 (ISO, 2001). Under the test conditions, LWC was 0.4 g/m^3. The air temperature was –5 °C and wind speed 4 m/s. The droplet size distribution in the icing tunnel has been calibrated by using The Cloud, Aerosol and Precipitation Spectrometer probe (CAPS), which can measures small particles between 0.61 and 50 µm by utilizing the light scattering principle (CAPS, Droplet Measurement Technologies, Boulder, CO, USA).

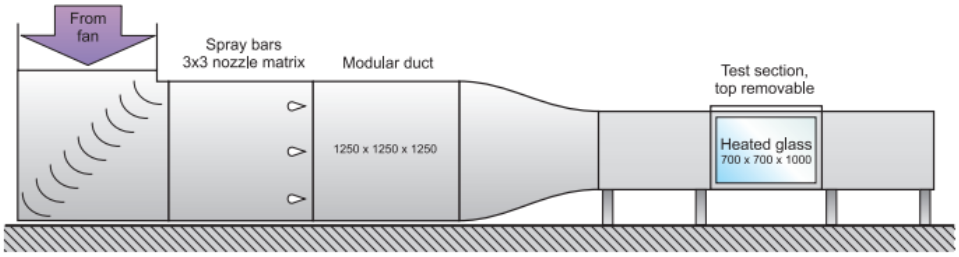

Figure 2. Icing wind tunnel schematic (VTT, 2016).

The cylinder in the experiments was weighted using electronic scales with precision of ±0.001 gram. The diameter of the cylinder after the ice accretion was measured using cooled calipers. Those measurements were conducted every 30 minutes. An example of ice shape obtained from the icing tunnel experiments is shown in Figure 3.

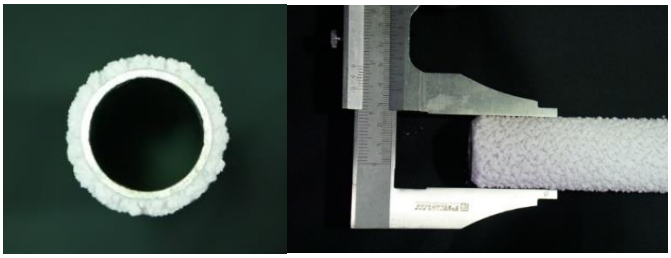

Figure 3: Ice shape from icing tunnel experimentations for 30 mm cylinder.

2.3 Numerical Setup

The multiphase CFD based numerical simulations were carried out using ANSYS FENSAP-ICE, which uses an Eulerian water droplet impingement solver. The general Eulerian two-phase model for viscous flow consists of the Navier-Stokes equations augmented by the droplets continuity and momentum equations (FENSAP User Manual):

$$\frac{\partial \alpha}{\partial t} + \vec{\nabla} \cdot \left(\alpha \overrightarrow{V_d}\right) = 0 \tag{10}$$

$$\frac{\partial \left(\alpha \overrightarrow{V_d}\right)}{\partial t} + \vec{\nabla}\left[\alpha \overrightarrow{V_d} \otimes \overrightarrow{V_d}\right] = \frac{C_D Re_d}{24K} \alpha \left(\overrightarrow{V_a} - \overrightarrow{V_d}\right) + \alpha \left(1 - \frac{\rho_a}{\rho_d}\right) \frac{1}{Fr^2} \tag{11}$$

where the variables α and $V_{d,a}$ are mean field values of, respectively, the water volume fraction and droplet velocity. The first term on the right-hand-side of the momentum equation represents the drag acting on droplets of mean diameter *d*. It is proportional to the relative droplet velocity, its drag coefficient C_D and the droplet Reynolds number:

$$Re_d = \frac{\rho_a d V_{a,\infty} \left\| \overrightarrow{V_a} - \overrightarrow{V_d} \right\|}{\mu_a} \tag{12}$$

$$K = \frac{\rho_d d^2 V_{a,\infty}}{18 L_\infty \mu_a} \tag{13}$$

Where L_∞ is the characteristic length of the object. In case of the cylinder, the characteristic length is cylinder radius. The second term represents buoyancy and gravity forces, and is proportional to the local Froude number:

$$\mathrm{Fr} = \frac{\left\| V_{a,\infty} \right\|}{\sqrt{L_\infty g_\infty}} \tag{14}$$

These governing equations describe the same physical droplet phenomenon as the Lagrangian particle tracking approach. Only the mathematical form in which these equations are derived changes, using Partial Differential Equations instead of Ordinary Differential Equations. The droplet drag coefficient is based on an empirical correlation for flow around spherical droplets, or:

$$C_D = (24/Re_d)\,(1 + 0.15Re_d^{0.687}) \quad \text{for} \quad Re_d \leq 1300$$

$$C_D = 0.4 \quad \text{for} \quad Re_d > 1300$$

The droplet local collision efficiency is calculated as follows:

$$\beta = -\frac{\alpha \overrightarrow{V_d} \cdot \vec{n}}{(\mathrm{LWC}) V_\infty} \tag{15}$$

where α is the local volume fraction (kg/m^3) and $\vec{n}$ is the surface normal vector. The total collision efficiency is an integration of local collision efficiencies over the surface area and is given as:

$$\beta_{\mathrm{tot}} = \frac{\int \beta \, dA}{L_\infty^2} \tag{16}$$

The ice density calculation procedures in FENSAP follows that given in the analytical model.

Detailed mesh sensitivity analysis were carried out to accurately determine the boundary layer characteristics (shear stress and heat fluxes), a *y*+ values of less than 1 is used near the cylinder wall surface. Number of mesh elements and *y*+ value was selected based upon the heat flux calculations, where a numerical check was imposed that the heat flux computed with the classical formulae dt/d*n* should be comparable with the heat flux computed with the Gresho's method.

3. Results and Discussion

3.1 Analytical Modeling

In this subsection the focus is to demonstrate the effect of the droplet distribution spectrum on cloud impingement parameters using the analytical procedure. The comparison is done using a series of graphs, which show the average value for each parameter, using algebraic value of all time steps. The purpose of this is to take into account the effect of the continued ice accretion process on respective values. Figure 4 shows the values for inertia parameter (*K*), normalized impact velocities at stagnation line in m/s (V_0), stagnation line local collision efficiencies (β_0), maximum impingement angles (θ) and overall collision efficiencies (*E*), respectively for all distributions. The "*spectrum averaged*" graphs present the spectrum averaged values of the respective parameter and how much each distribution contributes towards the average value with the exception of maximum impingement angles. The color code of Figures 4 and 5 should be read as follows: each unique color represents a single bin from any given distribution used from Figure 1 or Table 1. The right-hand side of Figures 4 and 5, which shows the "spectrum-averaged" values in a "stacked" way "stacks" the individual values of each bin, weighted by its respective LWC in order to obtain the "spectrum-averaged" values, where again, each unique color represents the contribution of individual bin towards the final value of a given cloud impingement parameter.

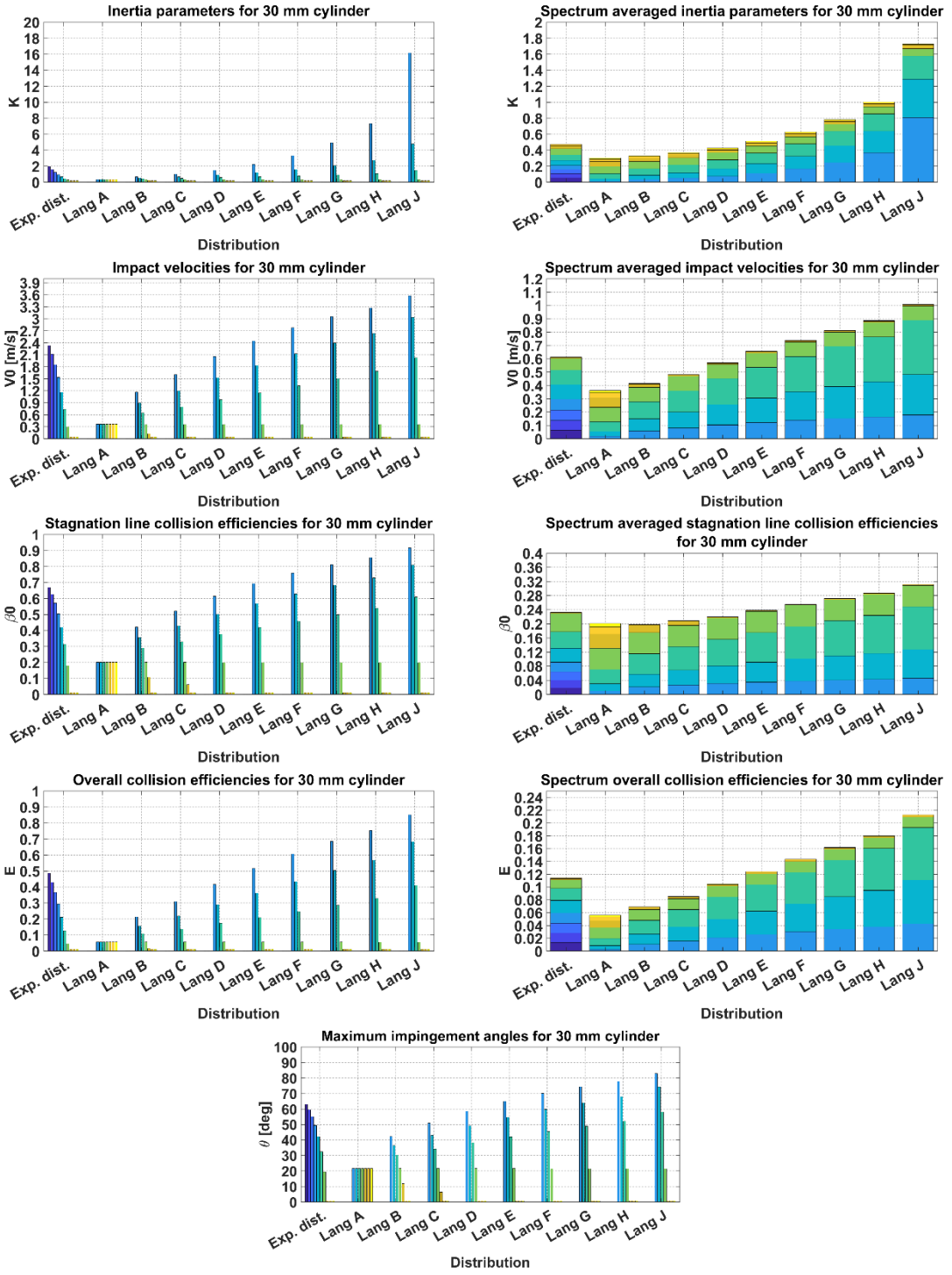

Figure 4. The values of cloud impingement parameters in the analytical model on per-bin basis (left) and spectrum-averaged values (right).

While it may be hard to estimate the change of any of the respective parameters during the process from the figures, the typical observed differences between start and end values for all parameters are within 2–3% for the ice accretion process under operating conditions from Table 1. However, for bins with smaller diameters, the limit of $K = 0.17$ is quickly reached and for distribution D and above the three smallest bins are consistently below the constraint value, meaning that limits of $E = \beta_0 = \nu_0 = \theta = 0.01$ are enforced and there is virtually no distinction between. However, the change in parameters of interest between larger droplet diameters in said distributions, when compared to the MVD value of 18.73 microns is of considerably larger magnitude, which smooths the impact of the constrained values to a large extent. In order to investigate the differences in values of cloud impingement parameters in a more concise manner, Table 4 lists the results of analytical calculations for all cloud impingement parameters with distributions from Figure 1 and Table 2 for MVD of 18.73 micron. In Tables 4 and 5 the "*Exp. dist. (E.d.)*" row refers to the results obtained using the experimental distribution from Figure 1, while the "*Experiment*" row refers to the experimentally measured values.

Distribution	Parameter							
	K	V_0 (m/s)	β_0	θ (deg)	E	M (g)	D (mm)	ρ (kg/m^3)
A	0.302	0.362	0.201	21.615	0.056	0.768	30.3	305.893
B	0.327	0.416	0.198	42.305	0.069	0.948	30.4	332.773
C	0.365	0.481	0.209	50.776	0.085	1.165	30.4	360.764
D	0.428	0.572	0.220	58.435	0.105	1.433	30.5	392.476
E	0.512	0.657	0.238	67.745	0.124	1.698	30.5	417.314
F	0.627	0.737	0.256	70.007	0.143	1.964	30.6	437.845
G	0.784	0.813	0.272	74.309	0.162	2.221	30.7	454.717
H	1.002	0.885	0.287	77.795	0.180	2.474	30.7	469.165
J	1.725	1.008	0.312	82.816	0.213	2.926	30.8	490.821
Exp. dist. (E.d.)	0.471	0.612	0.232	62.899	0.114	1.560	30.5	405.348
Experiment	0.458	–	–	–	**0.086**	**1.163**	–	–

Table 4: Spectrum weighted parameters values in analytical model.

As it is seen from Table 4, all cloud impingement parameters increase in their respective values with the increase of value in the droplet inertia parameter K, associated with change of the droplet distribution spectrum. The primary reason for said increase in the values of K is the significantly larger contribution to the spectrum-averaged values of droplet inertia parameter of individual bins with large droplet sizes, as it is seen from Figure 4. The resultant increase in values of the cloud impingement parameters is non-linear, primarily due to the structure of eq. (5) itself, and secondly, due to non-linear increase in the values of K associated with the change of the droplet distribution spectrum.

3.2 Numerical Analysis

The numerical simulations results for all distributions and bins are given in Figure 5, following the same methodology as was used in presenting the analytical results in Figure 5.

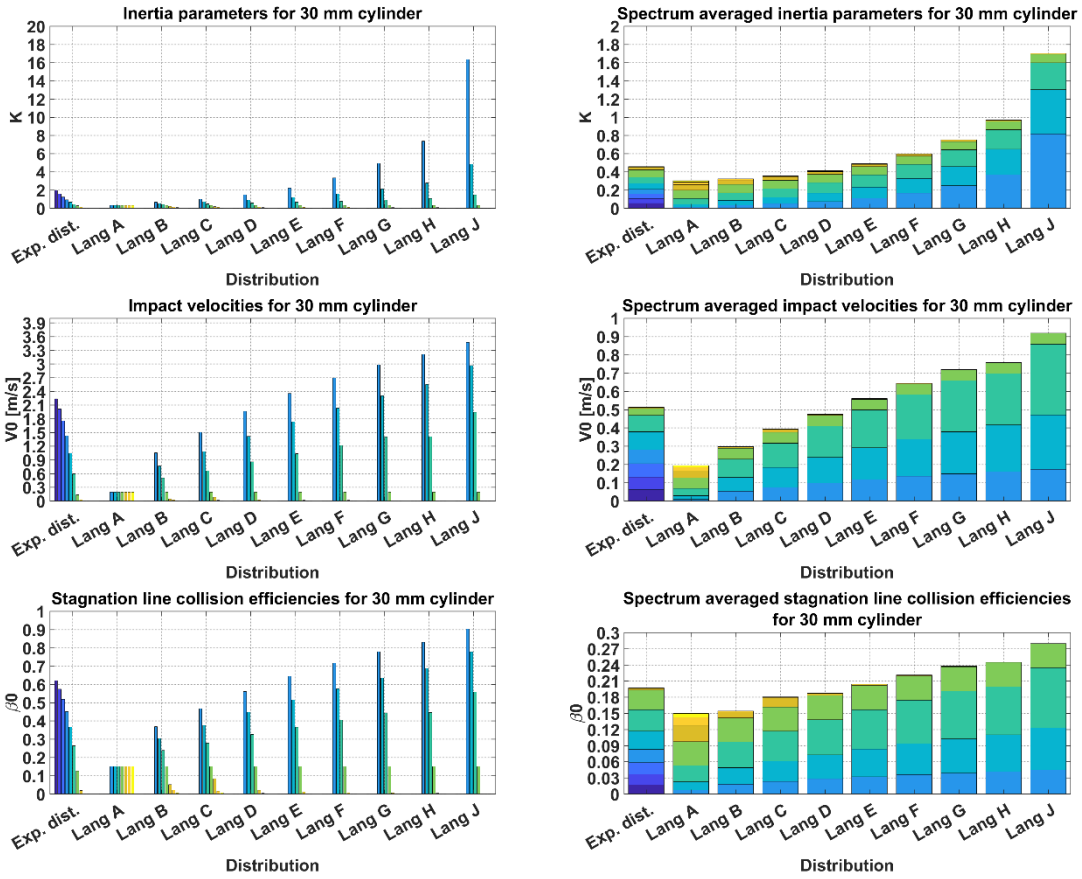

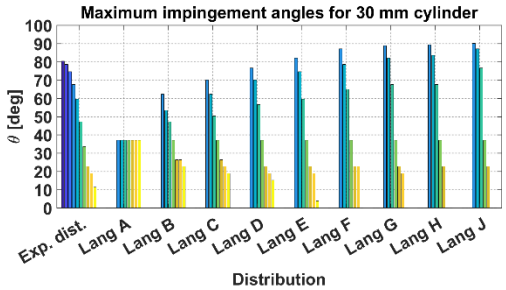

Figure 5: The values of cloud impingement parameters in the numerical model on per-bin basis (left) and spectrum-averaged values (right).

Numerical analysis show that in Figure 5, the maximum impingement angle remains unchanged for some droplets with different diameters, typically pertaining to smaller bins. The reason for this is that simulation data is output in terms of discrete "nodes" with coordinates and values of the respective parameter of that node, meaning that the precision is inherently limited to the amount of cylinder nodes in the simulation, as if any given property reaches value of zero in-between the nodes it will be rounded-up to the coordinates of the closest node. Furthermore, observe that in some of the cases, the reported value of the stagnation line collision efficiency is zero, while the impingement angle is not. The reason for this is the rounding to the three significant digits. Furthermore, since the values of inertia parameter in numerical simulations are not restricted in the same manner as in the analytical model, the values of impingement parameters can be below 0.01. Observe, that in numerical simulations the stagnation line collision efficiency and maximum impingement angles are equal to zero only for very small droplets, typically of the diameter of 5 microns or less, which gives a rough value of inertia parameter of 0.03. This differs from the assumptions of (Langmuir and Blodgett, 1944) and (Finstad, 1986) that those respective values can be equal to zero in cases of $K < 0.125$ and $K < 0.14$ respectively. Moreover, the impact velocities in the numerical simulations are never equal to zero. The total ice masses and the overall collision efficiency values after 30 minutes of ice accretion along cylinder with spectrum weighted data from Figure 5 are given in Table 5.

Distribution	**Parameter**					
	K	***V*₀ (m/s)**	**β₀**	**θ (deg)**	***E***	***M* (g)**
A	0.304	0.198	0.150	37.066	0.037	0.506
B	0.320	0.299	0.154	62.272	0.053	0.713
C	0.356	0.382	0.169	70.002	0.067	0.915
D	0.412	0.474	0.187	76.639	0.086	1.163
E	0.489	0.560	0.204	82.013	0.104	1.415
F	0.599	0.643	0.221	87.097	0.123	1.674
G	0.753	0.720	0.238	88.705	0.142	1.928
H	0.971	0.758	0.245	89.272	0.153	2.073
J	1.700	0.921	0.280	90.000	0.195	2.641
Exp. dist. (E.d.)	0.458	0.534	0.198	81.09	0.095	1.286
Experiment	0.458	–	–	–	**0.086**	**1.163**

Table 5: Spectrum weighted parameters values from numerical simulations.

Summarizing the results in Tables 4 and 5, the rotating cylinder in CFD simulations for all tested distributions exhibits smaller values in impact velocities, stagnation line and overall collision efficiencies, and by extension, the total accreted ice masses, while the values of maximum impingement angle are bigger than in the analytical model, even considering the potential impact of cylinder surface discretization and resultant nodes placement impact on maximum impingement angle in numerical simulations. Moreover, the use of modern CFD tools allows for in-depth investigation of a several concepts, not covered within the scope of the ISO 12494 model, such as viscous and boundary layer effects, liquid water content and droplet concentrations, vorticity and vorticity shedding, etc. As an example, Figure 6 shows droplet velocity magnitudes, impingement angles and local collision efficiencies for a few selected distributions.

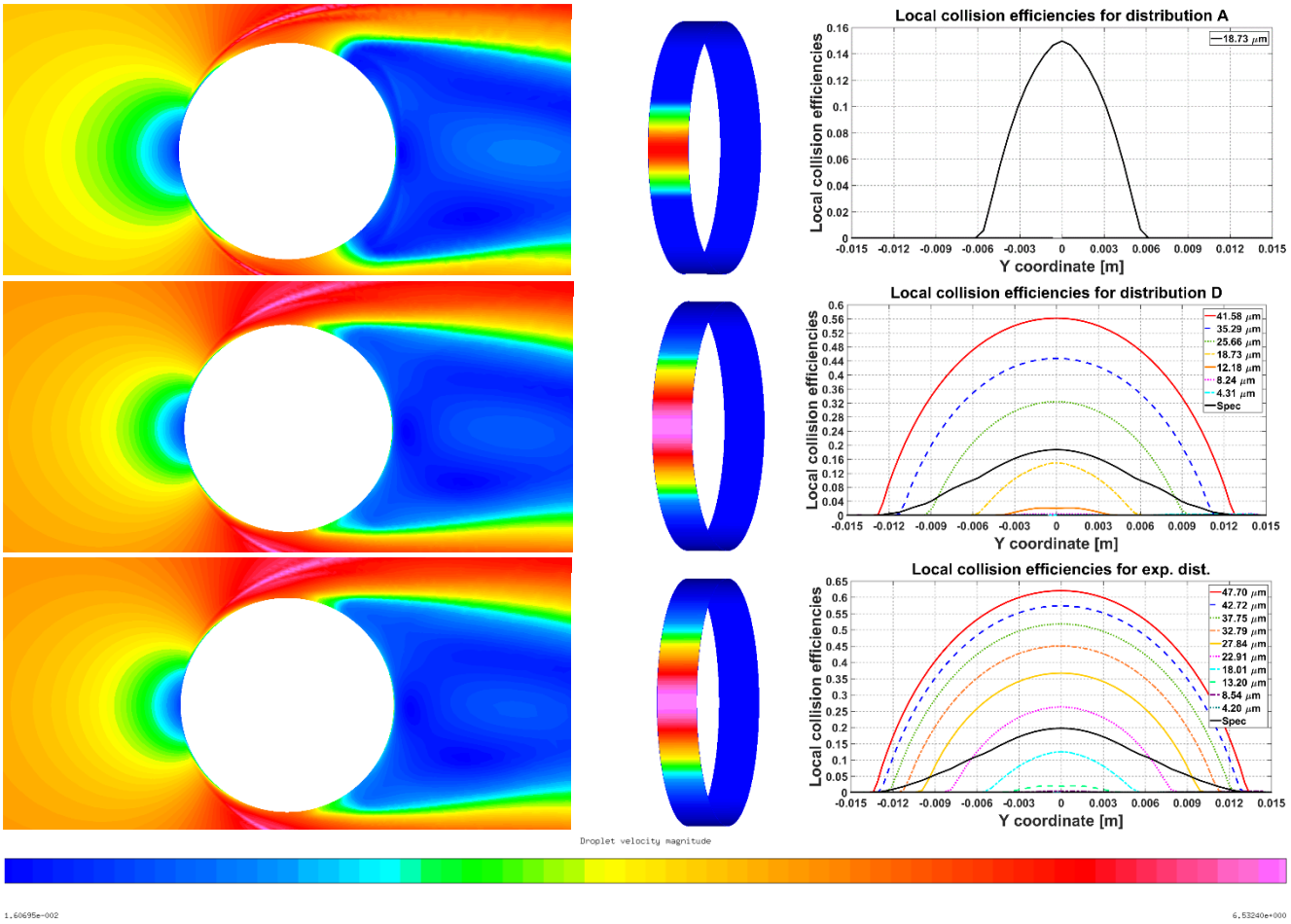

Figure 6: Droplet velocity magnitude (left), impingement angles (middle) and local collision efficiencies (right) for monodisperse (top), Langmuir D (middle) and experimental (bottom) distributions.

Figure 6 shows that the droplet behaviour changes extensively, depending on the droplet distribution spectrum used. Observe the significant difference in the maximum impingement angles, local collision efficiencies and much more "intricate" structure of the local collision efficiencies values, which directly correspond to the spectrum-weighted collision efficiencies, denoted as solid black line in Figure 6. Moreover, the maximum impingement angles seem to coincide well with the velocity minima from the velocity magnitude plots. In addition, the flow separation is much more clearly observed in said plots for experimental and Langmuir D distributions. As an overall, the numerical simulations are well suited for detailed studies of the droplet distribution spectrum effects and the ice accretion modeling in general, as multiple different cloud impingement parameters can be investigated and compared in detailed manner, which is not possible using analytical approach.

3.3 Comparison of Analytical, Numerical and Experimental Analysis

Summarizing the results from Tables 4 and 5, the analytical model tends to predict higher values of the stagnation line droplet collision efficiencies and impact velocities and as a result, the accreted ice masses. Contrary, the numerical results have higher values of the maximum impingement angles. Moreover, the relative increase in the values of the stagnation line collision efficiency and impact velocity, the overall collision efficiency and the total accreted ice mass, arising with the change of droplet distribution spectrum is also higher in the numerical results, while the relative increase in the values of the maximum impingement angle is higher in the analytical results. The higher values of the overall collision efficiency in the analytical results are expected to some extent due to the potential flow theory limitations, as discussed in (Yoon and Ettema, 1993).

In comparison, the experimental accreted ice mass is 1.163 grams, which results in an overall collision efficiency of 0.086. When comparing with analytical and numerical results from Tables 4 and 5 respectively, the closet fit distributions are distribution C for analytical results and distribution D for numerical results, respectively, with values of total ice mass and overall collision efficiency of 1.165 grams, 0.085 and 1.163 grams and 0.086, respectively. This match experimental results within the margin of error considering the rounding-up in calculations. Albeit unexpectedly the experimental distribution tends to produce higher values of overall collision efficiency and total ice mass in both analytical and numerical results,

being 1.560 grams and 0.114 respectively for analytical results and 1.286 grams and 0.095 for numerical results respectively. Some of this difference can be explained by restricting the inertia parameter in the analytical model and some possible uncertainty when it comes to the measured droplet spectrum in the tunnel. Moreover, the overestimation of overall collision efficiency can also be explained by the potential flow theory limitations, as was discussed in (Yoon and Ettema, 1993).

From Tables 4 and 5, it can be seen that results from monodisperse distribution are bad when compared to the experimental values. Monodispersed distribution failed to reproduce experimental values both in analytical and numerical calculations, and gave the lowest values for all the parameters across all distributions. However, based on the experimental verification of the Finstad et. al model done by (Makkonen and Stallabrass, 1987) along with discussion on some spectra properties done by (Langmuir and Blodgett, 1944), with recent investigation of droplet spectra effects by (Jones et. al., 2014) may suggest that this conclusion applies to cases with low values of inertia parameter only.

Furthermore, the governing theory from the ISO 12494 standard does not focus directly on the aspects of different cloud impingement parameters on ice accretion process other than the overall collision efficiency. While, as was discussed previously, the ISO 12494 theory and conducted experimental verification, such as in (Makkonen and Stallabrass, 1987) make the theory well developed and understood for the majority of typical icing situations and related engineering applications, especially those at higher wind speeds for long-term or extreme icing events the impact of those parameters, associated with the droplet distribution spectrum may be important in order to properly estimate the extreme or long term loads such icing conditions can exert on cylindrical structures, such as power lines or masts. Moreover, other factors, not accounted for in this study, such as surface roughness, sublimation and deposition, viscous and boundary layer effects may become prominent in cases where the inertia parameter is sufficiently low. However, the usage of the CFD tools as with this work, in addition to some recent results (Makkonen et al., 2018) show the CFD simulations are well suited for modeling of the ice accretion at the low values of *K*. As an example, a graphical comparison of the overall collision efficiency values in the analytical and numerical results is given in Figure 7. The practical meaning of Figure 7 is to display the difference in relative ice accretion values between the analytical and the numerical model in a concise manner.

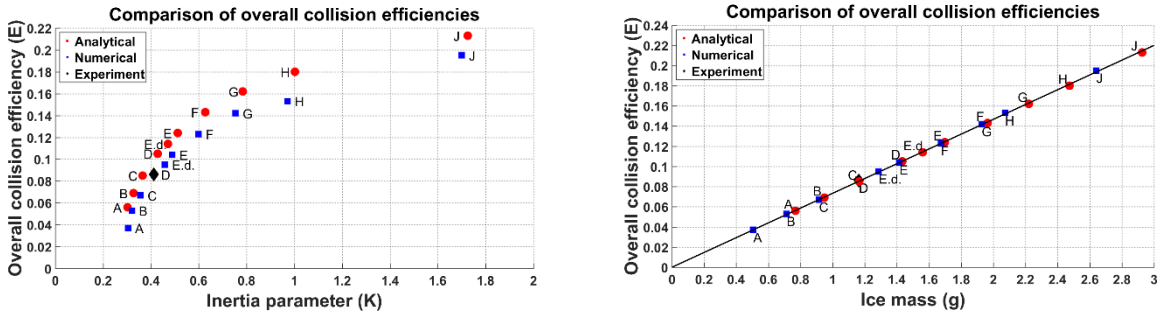

Figure 7. Comparison of analytical and numerical overall collision efficiency values. The distributions used are marked by the text. The numerical results are displayed below the reference line.

As it can be seen from the Figure 7, the monodisperse distribution (labelled "*A*") in both analytical and numerical cases tends to significantly underestimate the overall collision efficiency when compared to the actual experimental value (represented by the diamond). On the other hand, Langmuir D distribution yields good agreement with the experiment for the analytical case, and matches it exactly in the CFD simulations, while in the analytical results distribution C is very close to the experimental value of overall collision efficiency. The experimental distributions for both cases tends to overestimate the value of overall collision efficiency, however, for the CFD results the absolute error is approximately 0.01. Moreover, as it can be seen from Figure 7, the CFD and analytical results normally follow each other well, with the analytical results t having slightly higher values of the overall collision efficiency. This shows that modern CFD tools are well capable of simulating the ice accretion at low values of *K*, with $K \sim 0.4$ ($K \sim 0.3$ if calculated with MVD approximation) for the conditions in this study.

While it is difficult to properly judge the effects of surface roughness, due to associated issues with proper experimental measurements and modeling, both analytical and numerical, the viscous and boundary layer effects may be more explicable and easily observed in future experiments, provided strict control over experimental conditions is established and proper measuring devices are used. Overall, further experimental, analytical and numerical investigations into those aspects are deemed necessary in order to expand the understanding of connected terms on ice accretion process. In addition, the usage of the Langmuir D distribution as sort of a "first guess" distribution is recommended, as it is typically and successfully employed for aircraft icing studies (Bidwell, 2012), (Papadakis et. al, 2007), (Wright, 2008).

4. Conclusion

Within the scope of this paper a detailed analytical study along with a series of numerical simulations were performed for experimental data of ice accretion on a 30 mm cylinder. Results show that the droplet distribution spectrum change has a significant effect on the overall and local collision efficiencies, maximum impingement angles, droplet impact velocities, ice densities and ice mass accretion. The associated changes in the results are significant enough to cause the theory to either under estimate, be within the margin of error or significantly over estimate experimental results, depending on the droplet distribution chosen. Moreover, the numerical and analytical results tend to have some differences in the results, with tendency towards better agreement in the results of wider distributions with higher value of inertia parameter. This shows that care is needed when dealing with droplet distributions even with matching MVDs as those distributions do not have the same value of inertia parameter. The reported results are deemed valid for low values of droplet inertia parameter *K*.

Some of those differences can be explained using viscous, boundary layer and surface roughness effects, however, due to limitations of existing theory, particularly when it comes to inviscid flow assumption of the ISO model, further investigation in those aspects necessitates more experimental evidence in carefully controlled conditions, as it has been shown how a change in droplet distribution spectrum affects ice accretion on the cylinders, at lower values of droplet inertia. Overall, the further experimental, analytical and numerical investigations into those aspects at lower values of the droplet inertia parameter are deemed necessary in order to expand the understanding of connected terms on ice accretion process and performance of current icing theory in cases with low values of droplet inertia parameter. Out of those, the CFD simulations show good results for the low values of *K*, and as it has been shown in this work, allow for studying the variety of different parameters and their effect on the ice accretion process. For the low values of *K*, which correspond to the values of *E* being 0.10 or less the usage of the full droplet spectrum is recommended in calculations. In addition, based on the results of this and previous works the Langmuir D distribution is recommended as a first guess distribution.

Summarizing, the numerical model results produce the best agreement with the experimental results for narrower distributions B–E, while wider distributions tend to overestimate the accreted ice values. The analytical results tend to match experimental results well for distributions B–D, however, in general they tend to overestimate the accreted ice more than the numerical results, in particular for wider distributions F–J, however, this property can be exploited in the extreme value analysis of the icing events and ice maps generation.

Acknowledgment

The work reported in this paper is funded by the Research Council of Norway, FRonTLINES- project no. 245370 & IceBOX- project no 282403. Authors would like to acknowledge Mr. Timo Karlsson and Mr. Miko Tiihonen from VTT for providing icing wind tunnel experimental data used in this research work.

References

1. Bidwell, C.S., 2012, Particle Trajectory and Icing Analysis of the E3 Turbofan Engine Using LEWICE3D Version 3, NASA/TM–2012-217696, NASA
2. Cansdale, J., McNaughton, M., 1977. Calculation of Surface Temperature and Ice Accretion Rate in a Mixed Water Droplet/ice Crystal Cloud.
3. Finstad, K. J. 1986. Numerical and experimental studies of rime ice accretion on cylinders and airfoils. Ph.D. thesis. University of Alberta, Canada.doi:10.7939/R3N58CS1V.
4. Finstad, K.J., Lozowski, E.P., Gates, E.M., 1988a. A computational investigation of water droplet trajectories. Journal of Atmospheric and Oceanic Technology, 5, 160-170.doi:10.1175/1520-0426(1988)005<0160:ACIOWD>2.0.CO;2
5. Finstad, K.J., Lozowski, E.P., Makkonen, L., 1988b. On the median volume diameter approximation for droplet collision efficiency. Journal of the Atmospheric Sciences 45, pp. 4008–4012.doi: 10.1175/1520-0469(1988)045<4008:OTMVDA>2.0.CO;2
6. Howe, J.B. 1990. The rotating multicylinder method for the measurement of cloud liquid water content and droplet size. CRREL Report.
7. ISO 12494:2001(E), 2001. Atmospheric icing of structures. Standard. International Organization for Standardization. Geneva, CH
8. Jones, K.F., Thompson, G., Claffey, K.J., Kelsey, E.P, 2014, Gamma Distribution Parameters for Cloud Drop Distributions from Multicylinder Measurements. Journal of Applied Meteorology and Climatology, vol. 53, pp. 1606 – 1617. doi: 10.1175/JAMC-D-13-0306.1
9. Landau, L., and E. M. Lifshitz, “Fluid Mechanics,” Pergamon Press, pp. 96-98, 1959.

10. Langmuir, I., Blodgett, K., 1946. A Mathematical Investigation of Water Droplet Trajectories. Army Air Forces technical report 5418. Army Air Forces Headquarters, Air Technical Service Command.
11. Lozowski, E.P., Stallabrass, J.R., Hearty, P.F., "The icing of an unheated, non-rotating cylinder in liquid water droplet-ice crystal clouds," National Research Council of Canada, Ottawa, CANADA, Mechanical Engineering Report LTR-LT-96, Feb. 1979.
12. Lozowski, E.P., Makkonen, L., 2005. Fifty years of progress in modelling the accumulation of atmospheric ice on power network equipment, in: Proceedings of the 11th International Workshop on Atmospheric Icing of Structures.
13. Macklin, W.C., 1962. The density structure of ice formed by accretion. Quarterly Journal of Royal Meteorological Society, vol. 88 pp. 30–50.
14. Makkonen, L., 1984. Modeling of Ice Accretion on Wires. Journal of Applied Meteorology 23, 929-939. doi:10.1175/1520-0450(1984)023<0929:MOIAOW>2.0.CO;2
15. Makkonen, L., Stallabrass, J.R., 1987. Experiments on the cloud droplet collision efficiency of cylinders. Journal of Applied Meteorology 26, 1406-1411.doi:10.1175/1520-0450(1987)026<1406:EOTCDC>2.0.CO;2
16. Makkonen, L., 2000. Models for the growth of rime, glaze, icicles and wet snow on structures. Phil. Trans. R. Soc., Lond. A 2000 358 2913-2939; DOI: 10.1098/rsta2000.0690. Published 15 Nov. 2000
17. Makkonen, L., Zhang, J., Karlsson, T., Tiihonen, M., Modelling the growth of large rime ice accretions, CRST, 151 (2018), 133-137.
18. Papadakis M., Wong, S.-C., and Rachman, A, Large and Small Droplet Impingement Data on Airfoils and Two Simulated Ice Shapes, NASA/TM—2007-213959, October 2007
19. Ratvasky, T.P., Barnhart, B.P., Lee, S. Current Methods for Modeling and Simulating Icing Effects on Aircraft Performance, Stability and Control, NASA/TM—2008-215453, AIAA–2008–6204
20. Stallabrass, J.R., 1980. Trawler Icing: A Compilation of Work Done at N.R.C. (Givrage Des Chalutiers: Compilation Des Recherches Effectuees Au C.N.R.). Defense Technical Information Center.
21. Tsao, J.-C., Anderson, D.N, Additional Study of Water Droplet Median Volume Diameter (MVD) Effects on Ice Shapes, Conference: 42n AIAA Aerospace Sciences Meeting and Exhibit, At Reno, NV, Volume: AIAA 2004-0413, January 2004
22. http://www.vttresearch.com/Documents/Low%20Carbon%20Energy/Wind%20energy/Icing_Wind_Tunnel_02022016.pdf
23. Wagner, T. Modelling of Wind Borne Ice Accretion on Power Transmission Lines, Doctoral Thesis, University of Braunschweig, August 2010
24. Wiberg, B.D., Fujiwara, G.E.C., Woodard, B.S., and Bragg, M.B., "Large-Scale, Swept-Wing Icing Simulations in the NASA Glenn Icing Research Tunnel Using LEWICE3D," AIAA Paper 2014-2617, June 2014.
25. Wright, W., 2008, User's Manual for LEWICE Version 3.2, NASA/CR–2008-214255, NASA